Effect of sputtering power on the structural and optical properties of RF magnetron sputtered ITO films

1994 Semicond. Sci. Technol. 9 1242

(http://iopscience.iop.org/0268-1242/9/6/014)

Semicond. Sci. Technol. 9 (1994) 1242–1249. Printed in the UK

Effect of sputtering power on the structural and optical properties of RF magnetron sputtered ITO films

Wen-Fa Wu, Bi-Shiou Chiou and Shu-Ta Hsieh

Department of Electronics Engineering and Institute of Electronics, National Chiao Tung University, Hsinchu, Taiwan

Received 5 January 1994, accepted for publication 1 March 1994

Abstract. The structural and optical properties of RF magnetron sputtered ITO films without *in situ* substrate heating and post-deposition annealing are investigated. The structure and orientation of ITO films strongly depends on the energy of the sputtered particles arriving at the substrate. As the sputtering power increases from 15 to 100 W, the preferred orientation of the ITO film changes from (222) to (400). It is observed that the lattice constant of the film increases initially as sputtering power increases from 15 to 50 W and then decreases with further increase of sputtering power. The higher the sputtering power, the smaller the oxygen content of the film. The oxygen deficiency is used to explain the loss of transmittance or blackening of ITO films deposited at high sputtering power. Several material parameters, such as optical constants and energy gap, have been derived and discussed. The figure of merit of the films ranges from 81.3 to 117.6 Ω^{-1}.

1. Introduction

Transparent conductive indium tin oxide (ITO) films have been extensively used in a variety of electronics and optoelectronics applications because of their high transmission in the visible range, high infrared reflection and low electrical resistivity [1–8]. ITO films have been deposited by a variety of methods such as sputtering [1–3, 9–22], electron-beam evaporation [5, 6, 23, 24], spray pyrolysis [4, 7, 25] and screen-printing [26]. Magnetron sputtering can deposit films over large areas at rates comparable to electron-beam evaporation without the degree of radiation heating typical of thermal sources. The deposition rates of magnetron sputtering are higher than those for conventional radio-frequency (RF) sputtering and a wide range of materials can be deposited [27]. Magnetron sputtering is considered to be one of the best methods for preparing ITO films. High-quality ITO films prepared by magnetron sputtering have been reported [1, 9–15].

Although ITO films with both high electrical conductivity and high visible transmittance can be obtained, the blackening of ITO films was frequently observed during deposition of ITO films [6, 12, 22] and/or subsequent sputtering of dielectric films on ITO-coated substrates [28–30]. This made the transparent conductive ITO films unstable during operation. Kobayashi *et al*, in their work on ITO/silicon oxide/Si junction solar cells, attributed the darkening of ITO to the presence of metal indium [6]. Wu and Chiou [12] and Matsuoka *et al* [28] argued that the reduction of SnO_2 in ITO films resulted in the blackening of ITO. Fan and Goodenough associated the darkening with the formation of a second phase in the bulk of the films [22]. However, the mechanism for the blackening of ITO films is not clear. In this research, x-ray photoelectron spectroscopy (XPS) and x-ray diffraction techniques are employed in the study of blackening of ITO films. In addition, the effect of sputtering power on the structural and optoelectrical properties of the ITO films are investigated and discussed.

2. Experimental details

ITO films were prepared by using a commercial RF magnetron sputtering system (ION TECH, UK). The sputtering target was a 1 in hot-pressed oxide ceramic (90 wt% In_2O_3 and 10 wt% SnO_2, 99.99% purity) supplied by Superconductive Components, Inc., USA. The substrates employed were made of Corning 0211 glass, degreased ultrasonically in a dilute detergent solution, rinsed ultrasonically in de-ionized water and blown dry in N_2 gas before they were introduced into the chamber. The substrate was fixed directly above the target with a target-to-substrate distance of 5 cm and a mechanical shutter was attached to the target. The substrate temperature was measured with a thermocouple in intimate contact with the substrate.

The vacuum chamber was a stainless steel bell jar pumped by a conventional oil diffusion pump (Diffstak 250, Edwards, UK). High-purity Ar (99.999%) was

0268-1242/94/061242+08 $19.50

introduced through a mass flow controller after the vacuum chamber was evacuated to about 2×10^{-6} Torr. The gas pressure was monitored with a precision ionization gauge and was kept at 6.5 mTorr during deposition. The RF power (13.56 MHz) was introduced through an RF power supply (RF Plasma Products, Inc., USA) with an automatic matching network which could be tuned for minimum reflected power. The sputtering power employed ranged from 15 to 125 W and during sputtering the substrate temperature was between ~60 °C (15 W) and ~90 °C (125 W). Before deposition, the target was usually presputtered for 20–30 min to remove any contaminants and eliminate any differential sputtering effects.

Film thickness was measured with a stylus surface profiler. An x-ray diffractometer was used to identify the crystalline phase of the films. Chemical binding energy analysis was performed using an x-ray photoemission spectroscope (XPS; PERKIN PHI-590AM SAM/1905 ESCA, Massachusetts, USA) with an Mg K_α x-ray source. The microstructure of the films was analysed using a scanning electron microscope (SEM; Hitachi S-4000, Japan). The optical transmittance of the films were measured with an ultraviolet–visible–near-infrared spectrophotometer (Hitachi U-3410, Japan).

3. Results and discussion

Figure 1 gives the x-ray diffraction patterns for the as-deposited ITO films prepared at various sputtering powers. All the peaks can be assigned to the cubic bixbyite structure of In_2O_3. In the ASTM powder pattern for In_2O_3, the strongest peak is (222) and the third peak is (400) with a relative intensity $I(400)/I(222)$ of 0.3. In this study, at low sputtering power ($P = 15$ W), the two peaks (400) and (222) appear prominently, indicating the coexistence of ⟨100⟩ and ⟨111⟩ textures. At a power level between 25 and 75 W, the (222) peak disappears and the (400) peak becomes very strong, resulting in a preferred orientation in the ⟨100⟩ direction. However, as the sputtering power increases further, the (222) peak reappears, and the intensity of peak (222) is comparable to that of peak (400) at $P = 125$ W, as summarized in table 1. Kumar and Mansingh, in their work on RF sputtered ITO films, found that the structure and orientation of ITO films depended on the energy of the sputtered particles arriving at the substrate. They suggested that the thermalized sputtered atoms prefer to orientate in the (222) direction and the particles with higher energies prefer the (400) and (440) orientations depending on their energies [17]. Latz *et al* [1] and Suzuki *et al* [31]

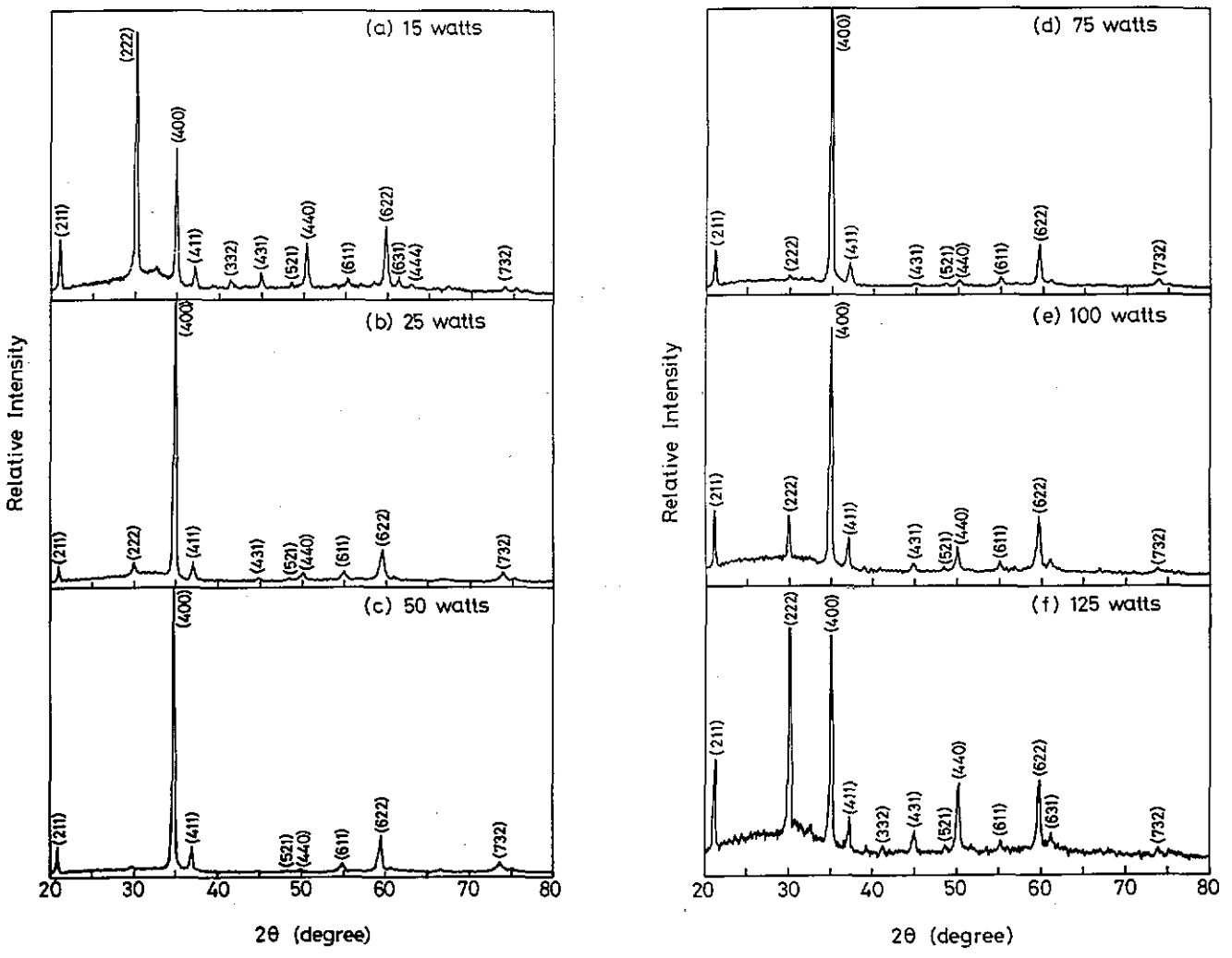

Figure 1. X-ray diffraction patterns for the as-deposited ITO films prepared at various sputtering powers.

Table 1. X-ray diffraction results for ITO films.

Sputtering power (W)	Lattice constant (Å)	Strongest peak	Relative intensity $I(222)/I(400)$[a]
15	10.173	(222)	1.842
25	10.224	(400)	0.043
50	10.281	(400)	Negligible
75	10.258	(400)	0.014
100	10.241	(400)	0.215
125	10.216	(400)	0.987

[a] In the ASTM powder pattern for In_2O_3, the relative intensity $I(222)/I(400)$ is 3.33.

observed a variation of the orientation from (222) to (400) with an increase in substrate temperature from ~100 to ~300 °C. In the present study, the trend that the preferred orientation of ITO films varies from (222) to (400) as sputtering power increases from 15 to 75 W is consistent with that reported previously [1, 17, 31]. However, further investigation is needed to explain the reappearance of the (222) peak at $P > 100$ W.

The cubic lattice constants, calculated from the most prominent peak in the x-ray diffraction patterns, are summarized in table 1. The lattice parameter ranges from 10.173 to 10.281 Å as compared with the ASTM value of 10.118 Å for bulk In_2O_3 [3]. There are several possibilities which might result in the lattice expansion of the ITO films. One is the replacement of In^{3+} ions with Sn^{2+} ions and/or the incorporation of Sn ions in the interstitial positions [3, 11]. The radii of the In^{3+}, Sn^{4+} and Sn^{2+} ions are 0.79 Å, 0.69 Å and 0.93 Å respectively [32]. The substitution of Sn^{2+} for In^{3+} would cause an expansion, as observed in the present study. The lattice constant increases from 10.173 to 10.281 Å as the sputtering power increases from 15 to 50 W and decreases with further increase of sputtering power. The mechanism which causes the increase of lattice parameter at $P \leq 50$ W is yet to be determined. The decrease of lattice constant with increasing RF power at $P > 50$ W can be attributed to the decrease of oxygen content at high sputtering power [12]. At high sputtering power, the substrate is being bombarded to a greater extent and the oxygen could be resputtered from the film during film growth. The oxygen is liberated and pumped off during the deposition process, resulting in a decrease in the oxygen content in the film. The decrease in the oxygen content enhances the presence of oxygen vacancies and results in the contraction of the lattice structure. One other possibility which causes the increase of lattice parameter is the residual stress in the sputtered film. However, further study is needed to reveal the contribution of the residual stress to the lattice expansion of the film.

Figure 2 gives the average transmittance, averaged over the wavelength range 0.45–0.8 μm, as a function of sputtering power. The average transmittance drops from 80% to 67% as the sputtering power increases from 15 to 125 W. XPS measurements were carried out to find chemical bonding states of ITO films and to explore

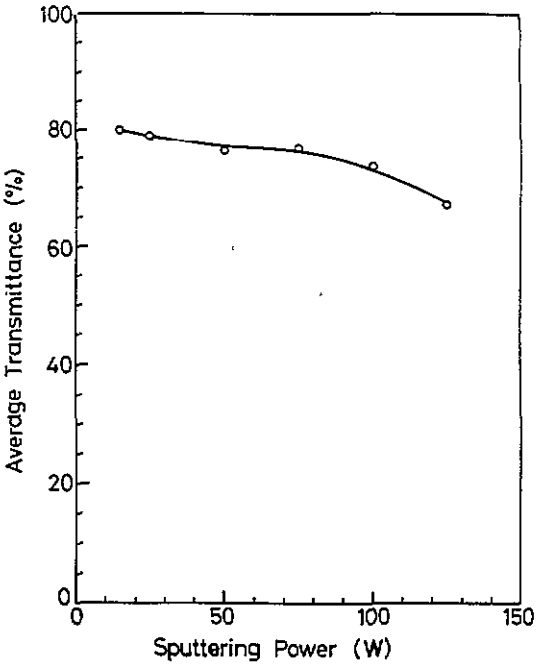

Figure 2. Average transmittance of the as-deposited ITO films, averaged over the wavelength range 0.45–0.8 μm, as a function of sputtering power.

the possible mechanisms for the loss of transmittance (or blackening) of ITO films prepared at high power. The In 3d, Sn 3d, and O 1s XPS spectra of the as-deposited ITO films prepared at various sputtering powers are shown in figures 3, 4 and 5 respectively. The position of the carbon 1s peak is taken as a standard (binding energy = 284.6 eV) to compensate for any charge-induced shifts. The obtained binding energies agree well with the values reported in the literature [5, 21–25, 28, 33, 34]. As shown in figure 3, the observed binding energies of the In $3d_{5/2}$

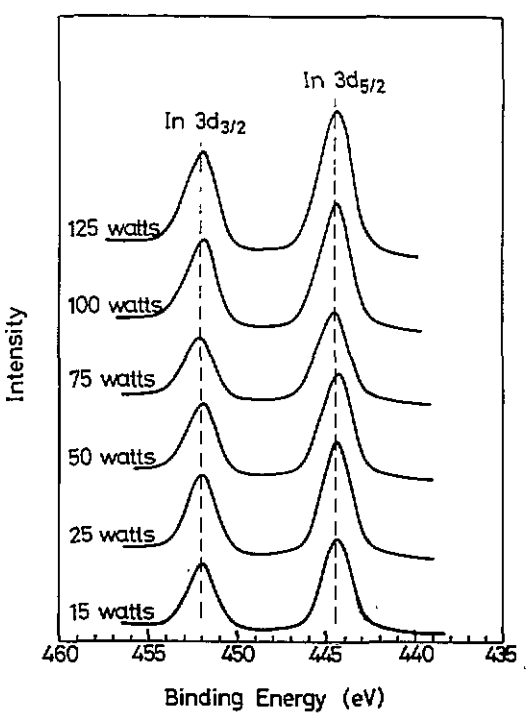

Figure 3. In 3d XPS spectra for the as-deposited ITO films prepared at various sputtering powers.

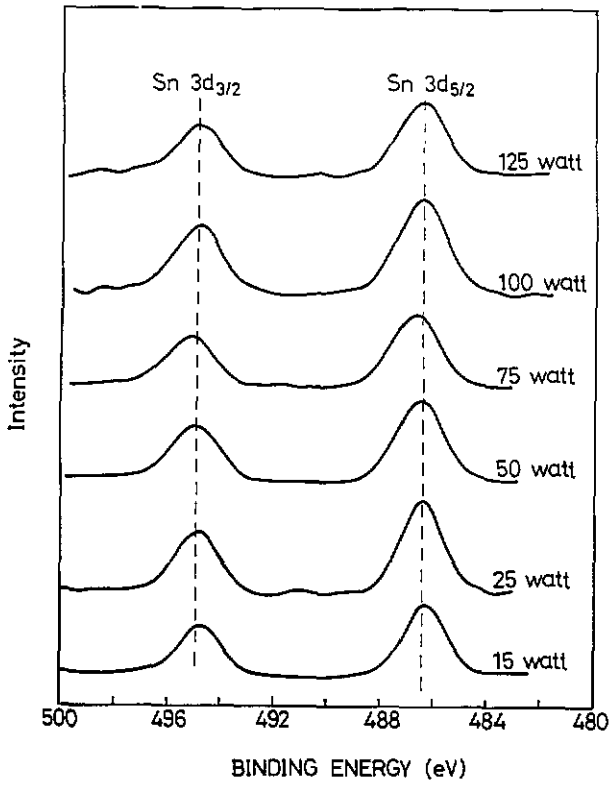

Figure 4. Sn 3d XPS spectra for the as-deposited ITO films prepared at various sputtering powers.

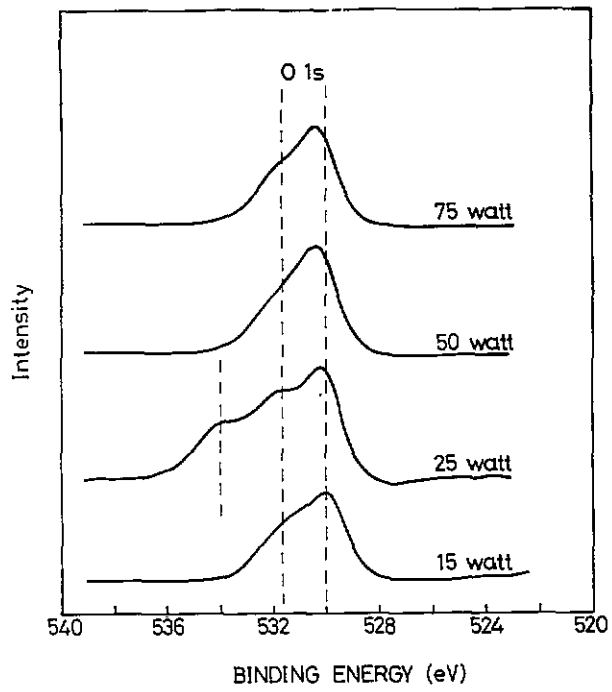

Figure 5. O 1s XPS spectra for the as-deposited ITO films prepared at various sputtering powers.

and In $3d_{3/2}$ levels are nearly the same, 444.4 and 452.0 eV respectively, for all samples. Since the extra electronic charge in the ITO films is trapped only at V_O (oxygen vacancies) and Sn centres, the In $3d_{3/2}$ and In $3d_{5/2}$ peaks should be insensitive to the loss of oxygen and to the Sn concentration [22]. It is reported in the literature [23, 33] that the In 3d peak for metal indium is observed at energies 0.4–1.4 eV lower than that for In_2O_3. Kobayashi *et al* [6] studied the darkening of ITO films prepared by electron-beam evaporation and suggested that darkening observed for the ITO films can be attributed to the presence of metal indium. However, no evidence exists in the present study to support the presence of metal indium in these ITO films. There is some asymmetry of the peaks, indicating that a multiple component may be present. Nelson and Aharoni [34] reported that the XPS In $3d_{5/2}$ peak can be resolved into two peaks which are separated by approximately 1.0 eV. The positions of the two resolved peaks in the In $3d_{5/2}$ spectra are located at 443.7 and 444.6 eV. They suggested that the lower-energy peak located at 443.7 eV corresponds to In^0 bonding state, specifically In–In bonds, and the higher-energy peak located at 444.6 eV corresponds to In^{3+} bonding state, specifically In_2O_3.

As shown in figure 4, almost the same Sn $3d_{3/2}$ and Sn $3d_{5/2}$ spectra are observed for the as-deposited ITO films prepared at various sputtering powers. Two peaks due to Sn $3d_{3/2}$ and Sn $3d_{5/2}$ are located at 495.0 ± 0.2 and 486.4 ± 0.2 eV respectively. Fan and Goodenough [22] reported that the Sn 3d peak for Sn^{2+} in SnO is observed at energy 0.5 eV higher than that for Sn^{4+} in SnO_2, whereas the Sn 3d peak for metal tin is observed at an energy 1.8 eV lower than the Sn^{4+} 3d peak. Thermodynamically SnO_2 is more stable than SnO and thus Sn^{4+} is thought to be the predominant state in the ITO films. Fan and Goodenough suggested that the darkening of the RF sputtered ITO films was caused by the formation of the Sn_3O_4 phase. However, no evidence for Sn_3O_4-like phase exists in the present work.

Figure 5 shows the XPS O 1s spectra of the as-deposited ITO films prepared at various sputtering powers. A shoulder appears on the higher energy of the main peak for the O 1s spectra in all samples. All the spectra (except $P = 25$ W) can be resolved into the two peaks at 530.0 and 531.7 eV, as shown by the broken line in figure 5. In_2O_3 crystallizes with a bixbyite C-type cubic rare earth sesquioxide crystal structure with space group $T_h^7 Ia3$ [22, 35]. Each indium atom is surrounded by six oxygen atoms at the corners of a distorted cube, with two vacancies at the two unoccupied corners. Fan and Goodenough suggested that the lower energy peak located at 530.0 eV corresponds to O^{2-} ions which have neighbouring In atoms with their full complement of six nearest-neighbour O^{2-} ions, and the higher energy peak located at 531.7 eV corresponds to O^{2-} ions in an oxygen-deficient region. Nelson and Aharoni proposed another possible explanation for the higher-energy peak and suggested that the higher-energy peak located at 531.7 eV may represent the existence of O–Sn bonds based on other group IV oxides [34]. As shown in figure 5, the main peak of the O 1s spectrum shifts to high binding energies at high sputtering power. It is believed that the magnitude of the shift to higher binding energies should vary with the oxygen deficiency associated with the nearest-neighbour In^{3+} ions. The O 1s spectrum

Table 2. XPS compositional analysis of ITO films.

RF power (W)	Atomic concentration (%)			Theoretical	
	X_{In}	X_{Sn}	X_O	$1.5X_{In} + 2X_{Sn}$	$X_O/X_{O(theoretical)}$
50	38.6	4.5	56.8	66.9	0.849
75	38.7	4.5	56.6	67.05	0.844
100	39.77	4.13	56.1	67.915	0.826
125	40.0	4.63	55.37	69.26	0.799

becomes very broad for the ITO film deposited at 25 W sputtering power, and another peak in addition to the two peaks already mentioned appeared at ~534.1 eV, as indicated in figure 5. It is suggested [23] that the 534.1 eV peak is attributed to oxygen atoms in the InOH species. It results from the existing OH groups on the surfaces of the samples which are caused by interaction with the surfaces of the samples under atmospheric conditions.

Compositional analysis is accomplished by dividing the peak areas by their respective atomic sensitivity factors and thus yields atomic per cent concentrations. Table 2 presents these XPS compositional analyses of ITO films deposited at different sputtering powers. This table also contains the theoretical estimate of the oxygen content ($X_O = 1.5X_{In} + 2X_{Sn}$, where X indicates atomic per cent) and compares this value with the experimental value. This comparison shows that a lack of oxygen is observed in all samples and the film becomes more non-stoichiometric as the sputtering power is increased during deposition. It suggests that the number of oxygen vacancies increases at high sputtering power and blackening is caused by the oxygen deficiency in the ITO films. These results agree well with those obtained from the x-ray diffraction experiment mentioned previously.

A block diagram of the algorithm for calculating the refractive index $n(\lambda)$ and the extinction coefficient $k(\lambda)$ of a thin optical layer from the transmission spectrum is shown in figure 6. A detailed description is given as follows.

According to Swanepoel's method [36], which is based on the idea of Manifacier *et al* [37] of creating the envelopes of interference maxima and minima in the transmission spectra, an approximate initial value of the refractive index of the film n_0 in the spectral region of medium and weak absorption, can be calculated by the expression

$$n_0 = [N + (N^2 - s^2)^{1/2}]^{1/2} \tag{1}$$

where

$$N = 2s\frac{T_M - T_m}{T_M T_m} + \frac{s^2 + 1}{2}. \tag{2}$$

Here T_M and T_m are the transmission maximum and the corresponding minimum at a certain wavelength λ, one being measured and the other calculated; s is the refractive index of the Corning 0211 glass substrate and a value of 1.523 is used. The basic equation for interference fringes is

$$4nd = m\lambda \tag{3}$$

where m is an even integer for maxima and an odd integer for minima, and d is the film thickness. Film thickness d was measured with a stylus surface profiler. The order of a given extremum m_0 can be estimated from equation (3) using d and the corresponding n_0. In addition, the values of m_0 can be determined by a simple graphical method based on equation (3). This expression can be rewritten for that purpose as

$$l = 4d\left(\frac{n_0}{\lambda}\right) - m_1 \tag{4}$$

where $l = 0, 1, 2, \ldots$ and m_1 is the first extremum. Therefore, plotting l against n_0/λ yields a straight line with slope $4d$ and intercept on the y axis of $-m_1$. From this plot the values of m_1 and hence each corresponding order of a given extremum m_0 can be estimated. The orders of m of the neighbouring extrema are in fact consecutive integers, even for the maxima and odd for the minima of the transmission. The final value of n for each extremum is obtained by substituting film thickness d and the corresponding exact integer values of m associated with each extreme point in equation (3). The value of the extinction coefficient k is obtained by the

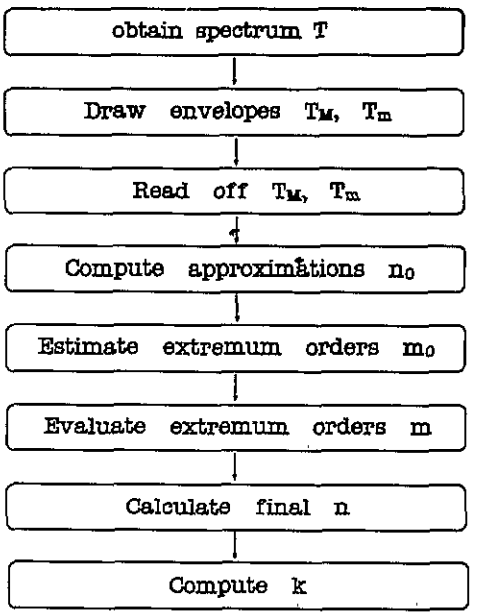

Figure 6. Block diagram of the algorithm for calculating $n(\lambda)$ and $k(\lambda)$ of a thin optical layer from the transmission spectrum.

following equations

$$E_M = \frac{3n^2 s}{T_M} + (n^2 - 1)(n^2 - s^2) \quad (5)$$

$$x = \frac{E_M - [E_M^2 - (n^2 - 1)^3(n^2 - s^4)]^{1/2}}{(n-1)^3(n - s^2)} \quad (6)$$

$$x = \exp\left(-\frac{4\pi k}{\lambda} d\right). \quad (7)$$

The refractive index versus wavelength for the ITO films deposited at different sputtering powers is shown in figure 7. The refractive index of the ITO film decreases with the wavelength λ, i.e. $dn/d\lambda < 0$. This is consistent with what one would expect from Kramers–Kronig analysis [9]. It is seen that the ITO films deposited at high sputtering power have a large value of refractive index. Figure 8 shows SEM micrographs of ITO films prepared at 15 and 125 W. The 125 W deposited ITO film has a smoother and denser structure than does the 15 W deposited one. It is argued that the denser structure is one reason for the larger refractive index of the film. The ITO films deposited at higher RF power have larger extinction coefficients, as shown in figure 9.

The transmission in the fundamental absorption region can be expressed by the equation

$$T \approx \exp(-\alpha d) \quad (8)$$

where T is the transmittance, α is the absorption coefficient and d is the film thickness. The absorption coefficient α for the direct allowed transition can be written as [10, 38]

$$\alpha = A(h\nu - E_g)^{1/2} \quad (9)$$

where $h\nu$ is the photon energy, E_g is the transition energy gap and A is a constant. Figure 10 shows the photon energy dependence of α^2 for two 8000 Å thick ITO films

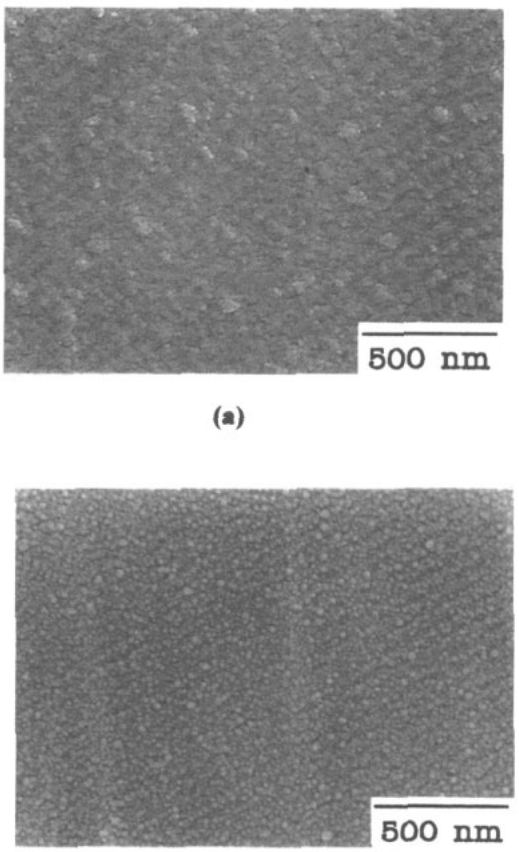

Figure 8. SEM microstructure of the ITO films deposited at (*a*) 15 W and (*b*) 125 W.

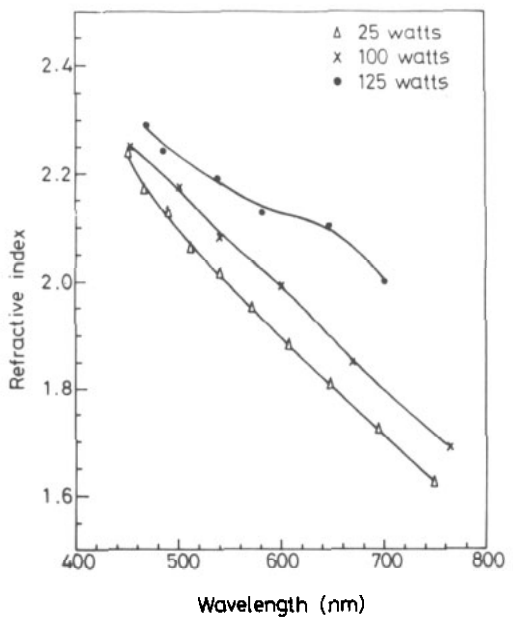

Figure 7. Refractive index n versus wavelength for the as-deposited ITO films prepared at various sputtering powers.

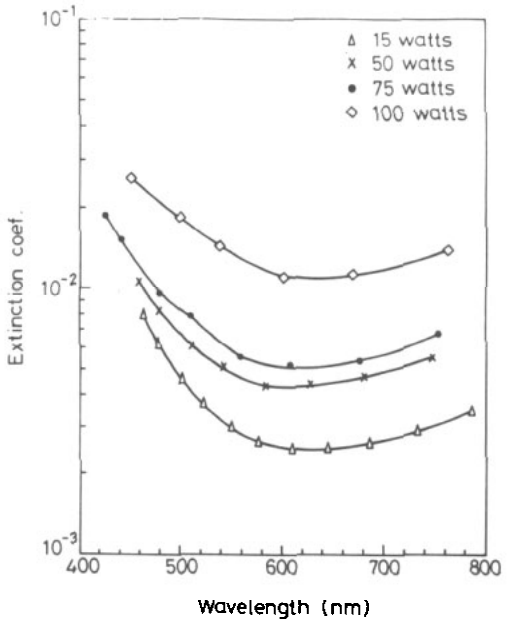

Figure 9. Extinction coefficient k versus wavelength for the as-deposited ITO films prepared at various sputtering powers.

Table 3. Comparison of ITO films prepared by different researchers.

Reference	Substrate temperature (°C)	Sputtering power (W)	Sheet resistance R_{sh} ($\Omega\,\square^{-1}$)	Transmittance ($\lambda = 5500$ Å), T (%)	Figure of merit ($\times 10^{-3}\,\Omega^{-1}$)	
					T^{10}/R_{sh}	T/R_{sh}
Present work	60	15	10.4	84.56	17.97	81.3
Present work	75	75	6.94	81.63	18.93	117.6
Present work	90	125	7.15	69.53	3.69	97.3
Latz *et al* [1]	300	600	19	87	13.1	45.8
Karasawa and Miyata [16]	Near room temperature	15	55	84	3.18	15.2
Ray *et al* [39]	370	200	4.5	90	77.5	200

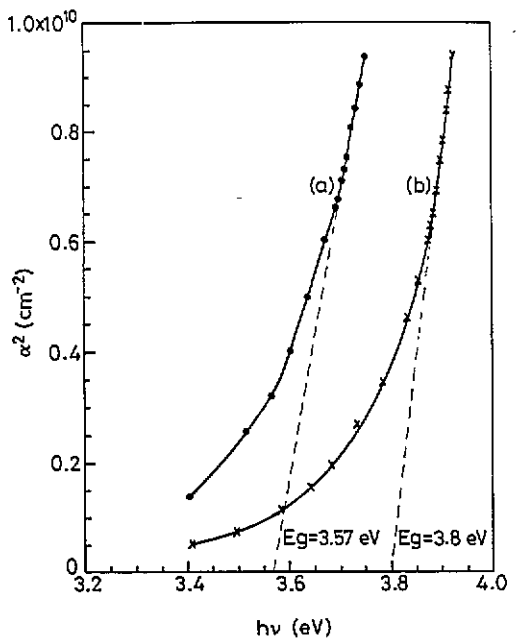

Figure 10. Square of the absorption coefficient α as a function of photon energy $h\nu$ for ITO films with a thickness of ~8000 Å. Sputtering power: (a) 25 W; (b) 75 W.

deposited at 25 and 75 W. Extrapolations of the straight regions of the plots to $\alpha = 0$ give the energy gap E_g. The E_g values obtained are 3.57 and 3.8 eV for films prepared at 25 and 75 W respectively. The carrier concentrations increase with the increasing RF power, they are 2×10^{20} cm^{-3} and 3×10^{20} cm^{-3} for films deposited at 25 and 75 W respectively [12]. Hence a larger energy gap is obtained for films prepared at higher power as predicted by the Burstein–Moss equation [9, 10, 38]

$$E_g - E_{g0} = \frac{\pi^2 h^2}{2m_r}\left(\frac{3N}{\pi}\right)^{2/3} \tag{10}$$

where N is carrier concentration, E_{g0} is the intrinsic bandgap, h is Planck's constant and m_r is the reduced effective mass.

Common to all transparent conductor applications is the need for optimizing the electrical and optical coating parameters. Ideally both the parameters should be as large as possible but their interrelationship usually excludes the simultaneous achievement of both criteria. To judge the performance of transparent conducting films, there are several ways to define the figure of merit. In table 3, two common definitions of figure of merit are adopted. The figures of merit for some ITO films prepared in this study are listed together with some of the values obtained by other researchers. The figures of merit of the low-power sputtered ITO films in this study are comparable to those reported in the literature. The small figure of merit for films prepared at 125 W is attributed to the blackening of the film.

4. Conclusion

The structural orientation of RF magnetron sputtered ITO films strongly depends on the sputtering power. Two peaks, (222) and (400), appear prominently in x-ray diffraction patterns of ITO films deposited at 15 W. The (222) peak disappears and the (400) peak becomes predominant as sputtering power increases from 25 to 75 W. The (222) peak reappears and the peak intensity of the (222) is comparable to the (400) peak at $P = 125$ W. In the sputtering power range 50 to 125 W, the lattice parameter of the as-deposited films is smaller for films deposited at higher power. The decrease of lattice parameter is attributed to the increase of oxygen vacancies in the film.

Blackening of ITO film is observed for films prepared at high power. XPS analyses of the films suggest that the oxygen deficiency results in the loss of transmittance of the films.

Sputtering power also affects the optoelectric parameters of the ITO films. The higher the sputtering power, the larger the refractive indices and the extinction coefficients. The transition energy gaps of 8000 Å thick ITO films are 3.57 and 3.8 eV for films deposited at 15 and 75 W respectively. The figures of merit of the films in this study are comparable to those reported in the literature.

Acknowledgment

This work is supported by the Chung-Shan Institute of Science and Technology (contract no CS 82-0210-D-009-016) and partly supported by the National Science Council of Taiwan (contract no NSC 82-0417-E009-395).

References

[1] Latz R, Michael K and Scherer M 1991 *Japan. J. Appl. Phys.* **30** L149
[2] Hoheisel M, Mitwalsky A and Mrotzek C 1991 *Phys. Status Solidi* a **123** 461
[3] Fan J C C and Bachner F J 1975 *J. Electrochem. Soc.* **122** 1719
[4] Ashok S, Sharma P P and Fonash S J 1980 *IEEE Trans. Electron Devices* **27** 725
[5] Haga K, Murakami A, Adachi K, Kumano M and Watanabe H 1992 *Japan. J. Appl. Phys.* **31** 925
[6] Kobayashi H, Ishida T, Nakamura K, Nakato Y and Tsubomura H 1992 *J. Appl. Phys.* **72** 5288
[7] Frank G, Kauer E and Köstlin H 1981 *Thin Solid Films* **77** 107
[8] Kido J, Nagai K and Okamoto Y 1993 *IEEE Trans. Electron Devices* **40** 1342
[9] Wu W F and Chiou B S 1993 *Appl. Surf. Sci* **68** 497
[10] Chiou B S and Hsieh S T 1993 *Thin Solid Films* **229** 146
[11] Chiou B S, Hsieh S T and Wu W F 1994 *J. Am. Ceram. Soc.* at press
[12] Wu W F and Chiou B S 1994 *Thin Solid Films* at press
[13] Chiou B S, Hsieh S T and Wu W F 1994 *Appl. Surf. Sci.* at press
[14] Shigesato Y, Takaki S and Haranou T 1991 *Appl. Surf. Sci.* **48/49** 269
[15] Martínez M A, Herrero J and Gutiérrez M T 1992 *Sol. Energy Mater.* **26** 309
[16] Karasawa T and Miyata Y 1993 *Thin Solid Films* **223** 135
[17] Kumar C V R V and Mansingh A 1989 *J. Appl. Phys.* **65** 1270
[18] Lee W-K, Machino T and Sughihara T 1993 *Thin Solid Films* **224** 105
[19] Shigesato Y, Hayashi Y, Masui A and Haranou T 1991 *Japan. J. Appl. Phys.* **30** 814
[20] Bosnell J R and Waghorne R 1973 *Thin Solid Films* **15** 141
[21] Hennig H, Heckner K-H, Hirsch D and Ladwig H 1982 *Phys. Status Solidi* a **74** 133
[22] Fan J C C and Goodenough J B 1977 *J. Appl. Phys.* **48** 3524
[23] Ishida T, Kobayashi H and Nakato Y 1993 *J. Appl. Phys.* **73** 4344
[24] Mori N 1993 *J. Appl. Phys.* **73** 1327
[25] Major S, Kumar S, Bhatnagar M and Chopra K L 1986 *Appl. Phys. Lett.* **49** 394
[26] Bessaïs B, Ezzaouia H and Bennaceur R 1993 *Semicond. Sci. Technol.* **8** 1671
[27] Vossen J L and Kern W 1978 *Thin Film Process* (New York: Academic)
[28] Matsuoka T, Kuwata J, Fujita Y and Abe A 1988 *Japan. J. Appl. Phys.* **27** L1199
[29] Panicker M P R and Essinger W F 1981 *J. Electrochem. Soc.* **128** 1943
[30] Chubachi Y and Aoyama K 1991 *Japan. J. Appl. Phys.* **30** 1442
[31] Suzuki K, Hashimoto N, Oyama T, Shimizu J, Akao Y and Kojima H 1993 *Thin Solid Films* **226** 104
[32] Kingery W D, Bowen H K and Uhlmann D R 1975 *Introduction to Ceramics* 2nd edn (New York: Wiley) p 85
[33] Hewitt R W and Winograd N 1980 *J. Appl. Phys.* **51** 2620
[34] Nelson A J and Aharoni H 1987 *J. Vac. Sci. Technol.* A **5** 231
[35] Elfallal I, Pilkington R D and Hill A E 1993 *Thin Solid Films* **223** 303
[36] Swanepoel R 1983 *J. Phys. E: Sci. Instrum.* **16** 1214
[37] Manifacier J C, Gasiot J and Fillard J P 1976 *J. Phys. E: Sci. Instrum.* **9** 1002
[38] Ohhata Y, Shinoki F and Yoshida S 1979 *Thin Solid Films* **59** 255
[39] Ray S, Banerjee R, Basu N, Batabyal A K and Barua A K 1983 *J. Appl. Phys.* **54** 3497